A Fundamental Understanding of the Dependence of the Laser-Induced Breakdown Spectroscopy (LIBS) Signal Strength on the Complex Focusing Dynamics of Femtosecond Laser Pulses on Either Side of the Focus

Craig A. Zuhlke,[a,*] John Bruce III,[a] Troy P. Anderson,[a] Dennis R. Alexander,[a] Christian G. Parigger[b]

[a] *Electrical Engineering Department, 209N WSEC Link, University of Nebraska, Lincoln, NE 68588 USA*
[b] *The Center for Laser Applications, The University of Tennessee Space Institute, Tullahoma, TN 37388 USA*

We correlate the focusing dynamics of 50 femtosecond (fs) laser radiation as it interacts with a silicon sample to laser-induced breakdown spectroscopy (LIBS) signal strength. Presented are concentric ring-shaped variations in the electric field in the prefocus region due to lens aberrations and nonsymmetry between the prefocus and post-focus beam profile as a result of continuum generation, occurring around the focus. Experimental results show different signal trends for both atmospheric and vacuum conditions, attributed to the existence of a continuum for the former. Lens aberrations effects on the LIBS signal strength are investigated using a plano-convex spherical lens and an aspherized achromatic lens. High-resolution scanning electron micrographs of the silicon surface after ablation, along with theoretical simulations, reveal the electric field patterns near the focus. The research results contribute to fundamental understanding of the basic physics of ultrashort, femtosecond laser radiation interacting with materials.

Index Headings: **Femtosecond LIBS; fsLIBS; Laser-induced breakdown spectroscopy; LIBS; Continuum; Interference.**

INTRODUCTION

A well-known concern with laser-induced breakdown spectroscopy (LIBS) is that experimental results often vary from one group to another and even within a single lab from day to day. With femtosecond LIBS it should be taken into consideration that the focusing dynamics of femtosecond laser pulses are complex. The complexity is in the form of nonuniform electric field distributions as a result of lens aberrations inherent in the focusing optics commonly used with LIBS, as well as nonlinear atmospheric breakdown processes that occur near the focus. When a laser pulse is focused using a lens that causes spherical aberrations, the electric fields exhibit distortions in the form of concentric rings of varying intensity. These distortions are only present in the spatial region between the focusing lens and the focal volume (prefocus). Evidence of these concentric ring distortions has been demonstrated through direct measurement of the electric field of focused femtosecond pulses by Bowlan et al.[1,2] The same work by Bowlan et al. reveals that in the post-focus spatial region the electric field distribution has a Gaussian distribution related to the profile of the input beam without concentric ring distortions.

Received 18 November 2013; accepted 28 April 2014.
* Author to whom correspondence should be sent. E-mail: czuhlke@unl.edu.
DOI: 10.1366/13-07387

Although the variations in the electric fields across the profile are not present beyond the focus, there are other processes that further affect the profile in this region. For example, when focusing femtosecond radiation, high peak intensities near the focus result in ionization of the air molecules. This ionization leads to the formation of an air plasma and continuum light generation.[3–5] The generation of continuum light from femtosecond radiation is not fully understood, but some theories include self-phase modulation, self-steepening, or cross-phase modulation.[6,7] By nature, this continuum light shows broadband distributions.[5,8] Results obtained with an auto-correlator device (not included here) indicate that the continuum light also occurs at the femtosecond time scale, similar to results obtained for spectrally broadened pulses in femtosecond laser filamentation.[5,9] Figure 1b shows an example spectrum of this typical continuum, along with the original spectrum of the pulses from the laser (Fig. 1a). The continuum spectrum is unstable; our results indicate that the spectrum shifts rapidly with time at a single spatial location. Thus, the spectrum shown in Fig. 1b is representative and can change from shot to shot even with the exact same time delay at which the spectrum is being recorded.

Furthermore, the continuum light expands at a higher rate than the normal Gaussian beam expansion as a result of different wavelengths and index of refraction changes.[3–5] This difference in expansion is visible in the optical image in Fig. 1c. We obtained this image (sometimes referred to as the bull's eye pattern[10]) by imaging the scattering from a black object that is located about 200 mm post-focus. This nonuniform spatial expansion of continuum and the original laser beam wavelengths results in a nonsymmetric beam waist as a function of distance on either side of the focus, and, as discussed in this paper, also leads to nonsymmetry in the femtosecond LIBS signal strength on either side of the focus. Figure 2 illustrates the full focusing dynamics of femtosecond pulses in air.

This work elaborates our efforts to understand how these complex focusing dynamics affect the LIBS signal strength as a function of sample location relative to the focus.[11] Experiments were completed to combine a map of the LIBS signal strength as a function of sample location relative to the focus with scanning electron microscope (SEM) images of the corresponding ablation craters. Results presented here elucidate the complexity

0003-7028/14/6809-1021/0

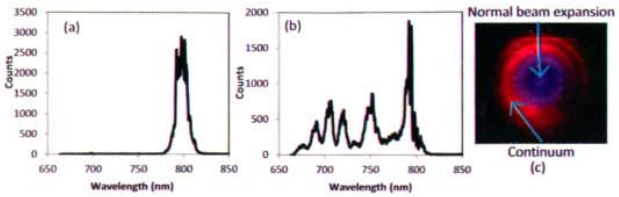

FIG. 1. Spectrum of (**a**) pulses directly out of the laser, and (**b**) the continuum light after the focus of the pulses (this is not stable, it varies rapidly over time in the same location). (**c**) Image of the normal pulse expansion and continuum light incident on a black surface about 200 mm beyond the focus.

of the LIBS signal and explain why LIBS results can vary from group to group and even from one day to another in a research laboratory (laser chirp, pulse length, wavelength, etc. can vary slightly from day to day); these results also emphasize the need for tightly controlled parameters for research using LIBS.

Experimental Arrangement. Figure 3 illustrates the experimental arrangement for our work. The laser was a Spectra Physics Spitfire, Ti:Sapphire system that uses chirped pulse amplification. The system is capable of producing 1 mJ, 50 fs, linear polarized pulses centered at 800 nm at a 1 kHz repetition rate. Through the use of a fast shutter, the number of pulses incident on the sample can be controlled down to individual pulses. The pulse length and chirp were monitored using a frequency resolved optical gating instrument from Positive Light (Model 8-02). The sample position relative to the focal volume was controlled using Melles Griot Nanomotion II translation stages with three axes of motion, 10 nm resolution, and 1 μm accuracy.

The pulses were focused onto the sample using two different lenses. The first was a 25 mm diameter, 40 mm focal length plano-convex (PC) spherical lens made of BK7 glass (Edmund Optics NT47-345). The second lens was a 25 mm diameter, 40 mm focal length aspherized achromatic (AA) lens (Edmund Optics NT49-664). These lenses were chosen to be a matched pair in terms of focal length, while the PC lens contains aberrations and the AA lens is corrected to minimize the effects of spherical and chromatic aberrations.

The LIBS signal was collected using a 50 mm diameter collection optic to focus the light into a fiber optic cable that delivers the light to the spectrometer. The spectrometer was an Andor Mechelle 5000 echelle-style spectrometer with an intensified charge-coupled device

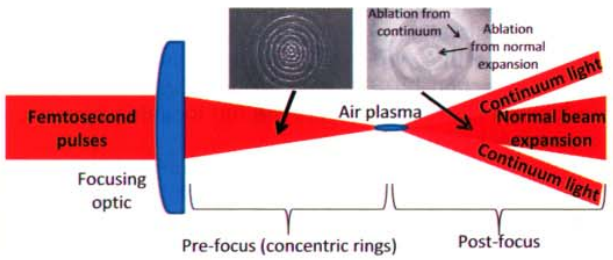

FIG. 2. Diagram of the dynamics occurring during the focusing of femtosecond pulses. The top images are scanning electron microscope (SEM) images of ablation craters created with the sample located in the marked region relative to the focus.

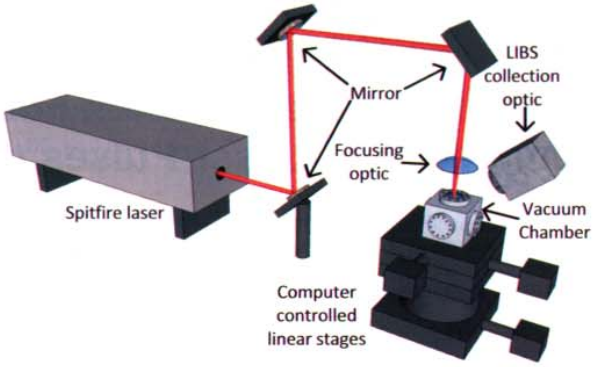

FIG. 3. Experimental setup.

(ICCD) that allows for fast gating of the detector element. A beam pickoff for the laser provides signal to a photodiode that triggers the ICCD in the spectrometer. Accounting for signal delays in both the triggering coaxial cable and the optical delay introduced with the fiber optic cable as well as the ICCD turn on time means that the spectrometer starts collecting signal 38 ± 2 ns after the laser pulse arrives on the sample. The ICCD within the spectrometer was set to collect light for 500 ns after it was triggered, which is effectively the full lifetime of the laser-induced plasma produced using this setup.

The material used in this work was undoped silicon with a polished face. For part of the research the sample was loaded in a small vacuum chamber that was mounted on the translation stages and was evacuated to 2 Pa (1.5×10^{-2} Torr). All the presented LIBS research uses the 288.1579 nm Si I emission line, which is the dominant emission line for Si that is within the range of our spectrometer. For all LIBS experiments, a pulse energy of 750 μJ was incident on the sample. Silicon was chosen for this research because of the initial optically smooth surface and fast solidification, which result in a clean ablation pattern mirroring the incident electric field intensity distribution.

Experimental Details. Prior to conducting our experimental work, computations were completed in order to verify the beam size/lens combination that, considering spherical aberrations, would result in concentric ring distortions in the electric field intensity of the prefocus spatial region. The theoretical modeling was completed for a monochromatic Gaussian beam with a beam waist of 5.77 mm, at a wavelength of 800 nm, focused using the 40 mm focal length plano-convex lens described in the experimental setup section. The simulations modeled the evolution of the beam profile through the focus by evaluating the Fresnel diffraction integral using the Debye integral method.[12,13] It should be noted that the manufacturer specified that the focal length of 40 mm is designated for 633 nm light, while the actual focal length for 800 nm light is just beyond 40 mm. The theoretical electric field distribution for the beam propagating in the *z*-direction is shown in Fig. 4, which is a cross section of the electric field intensity. These representative theoretical results serve to verify the concentric ring distribution in the electric field intensity prefocus and the Gaussian

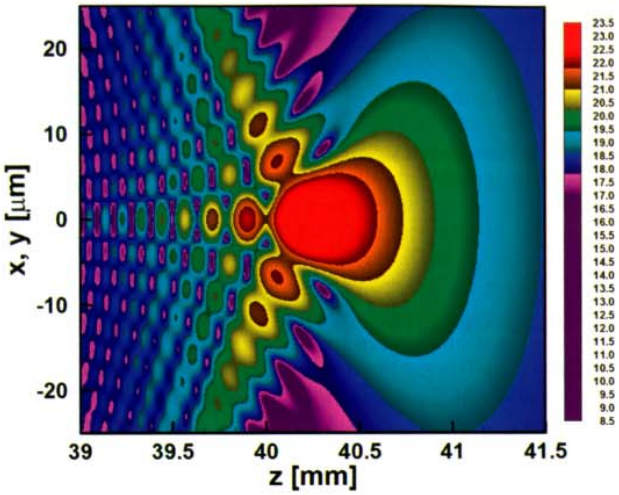

FIG. 4. Theoretical modeling of electric field distribution as a function of focus for an 800 nm Gaussian beam focused with the 40 mm focal length plano-convex lens that shows spherical aberrations.

distribution post-focus for the lens/beam combination used in this work.

With knowledge of the complex electric field distribution through the focus in hand, we conducted experiments to interrogate effects on the LIBS signal strength. In the experimental part of the research, the LIBS signal strength was collected as a function of sample location relative to the focal volume for the two different kinds of lenses. Experiments were also conducted with the sample (and focal volume) inside a vacuum chamber, where the reduced concentration of air molecules diminishes continuum generation, in order to understand the extent to which continuum generation affects the LIBS signal strength. The vacuum work was only completed using the PC lens.

Meticulous care was taken to determine the relative vertical stage position at which the sample surface was precisely at the focus of the sample. In order to define a "true" focus, the pulse energy was reduced to the point that the silicon surface was only modified when the sample surface was at the focal point of the pulses. At this pulse energy, single laser pulses were incident on the sample at different locations, with the sample surface passing through the focus in 10 μm steps. As a result,

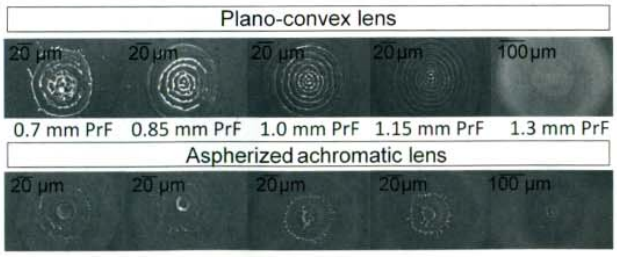

FIG. 5. SEM images of the resulting ablation spots produced during LIBS data collection. Each column is at the same relative sample location specified using the locations labeled between the rows (PrF, prefocus). The top row was produced using the PC lens, and the bottom row using the AA lens.

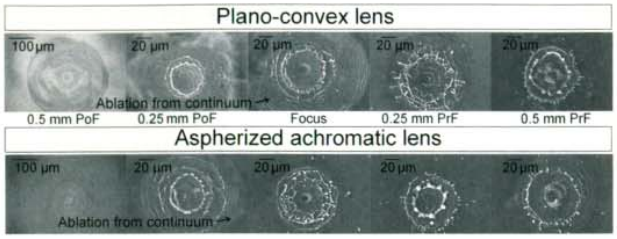

FIG. 6. SEM images of the resulting ablation spots produced during LIBS data collection. Each column is at the same relative sample location specified using the locations labeled between the rows (PrF, prefocus; PoF, post-focus). The top row was produced using the PC lens and the bottom row using the AA lens.

there was only a 50 μm range where any modification to the silicon surface could be visualized in the SEM. This position in the *z* direction was then defined as the "true" focus for the system.

Equal care was taken to ensure proper lens alignment. Due to the ablation dynamics associated with femtosecond pulses, the electric field intensity distributions of the pulses during ablation become frozen in the sample surface, and therefore the ablation spot becomes a map of the distribution. We observed that the method of using a back reflection off the lens through a pinhole was not always an adequate alignment procedure, resulting in nonsymmetric ablation patterns. As a more precise alignment procedure, ablation spots were made with the surface of the silicon sample prefocus where the concentric ring structure was visible in the ablation spot. A series of ablation spots was produced making slight lens adjustments between spots. The spots were then viewed in the SEM, and a trend toward uniform rings was sought. This trend was recorded using the SEM images, and the process was repeated until a uniform ring pattern in the ablation spot was achieved. The careful alignment results in the symmetric ring pattern that can be seen in Fig. 5.

RESULTS AND DISCUSSION

In the prefocus region, there is a significant difference in the electric field distributions as a function of the *z*-position around the focus when comparing the two lenses used. For the PC lens, concentric ring distortions (frozen melt patterns) in the electric field intensity distribution are present at the prefocus as a result of the lens aberrations, and the number of rings decreases moving closer to the focus. With the AA lens, these concentric ring patterns are almost nonexistent. This difference in the chosen lenses used to focus the femtosecond pulses is evident in Fig. 5, which is a series of SEM images of ablation spots for each lens in the prefocus region. Notice the AA lens is not completely aberration free, so there are still some non-Gaussian variations visible in the melt patterns.

The AA lens results in a lower deviation angle for the generated continuum light than the PC lens, which is likely related to the cleaner focus of the AA lens. Ablation from the generated continuum light can be seen around the fringes of some of the ablation spots in the series of SEM images on either side of the focus in Fig. 6. Notice that with the PC lens, the continuum

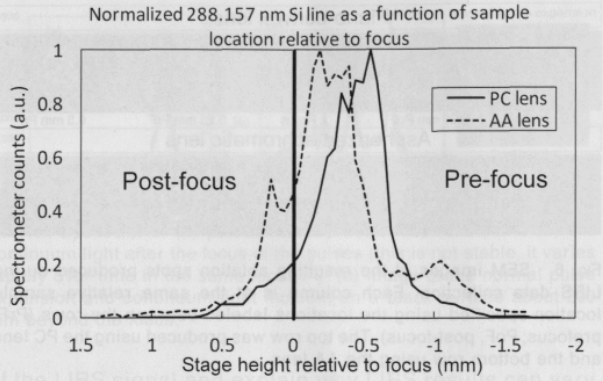

FIG. 7. Comparison of LIBS signal strength for a PC lens compared with an AA lens both with a focal length of 40 mm.

generation is well established at the focus and expands at a much higher rate than with the AA lens.

The differences in the focusing dynamics between the AA and PC lenses leads to a different dependence of the LIBS signal strength on the sample location relative to the focus when comparing results obtained using the two lenses. This difference is illustrated in Fig. 7, which is a comparison of the LIBS signal as a function of sample location relative to the focus for the PC and AA lens. The plot is of the 288.157 nm Si line, each point is the median LIBS signal collected from 50 individual shots, and the data sets are normalized for a more direct comparison. Notice that the LIBS signal from the PC lens has only a single peak, while the AA results in three peaks, each of which will be discussed in detail. Also note that the peak for the AA lens is shifted closer to the focus when compared with the PC lens. This shifting of the peak position is the result of a combination of the cleaner focus and the lower divergence angle of the generated continuum light using the AA.

Further insight into the shape of the LIBS signal curve for the PC lens can be gained by comparing the LIBS signal strength at specified heights to the imprinted electric fields seen in the ablation patterns. Figure 8 includes typical SEM images of ablation spots matched to the corresponding LIBS data points as a function of sample location relative to the focus (the focus is at zero on the plot). The series of ablation images shows the full progression of the focusing dynamics. Starting with the sample located above the focus (right column of images), the concentric ring pattern distribution can be observed. Moving below the focus (lower left image) there is no ring pattern, but ablation from the continuum can be seen. From Fig. 8, we see that the LIBS signal has a single peak, which occurs prefocus and continuously drops off in intensity as the sample is moved through and beyond the focus. It is apparent from the SEM images that when moving from the prefocus toward the focus, the initial increase in LIBS signal occurs in the same region where the concentric ring pattern begins to become less distinct and begins to disappear. It is currently unclear whether the increase in LIBS signal is related to the transition out of concentric ring structure or this increase is simply due to the increase in fluence approaching the focus. Upon close inspection of the ablation spots, it is clear that moving away from the lens

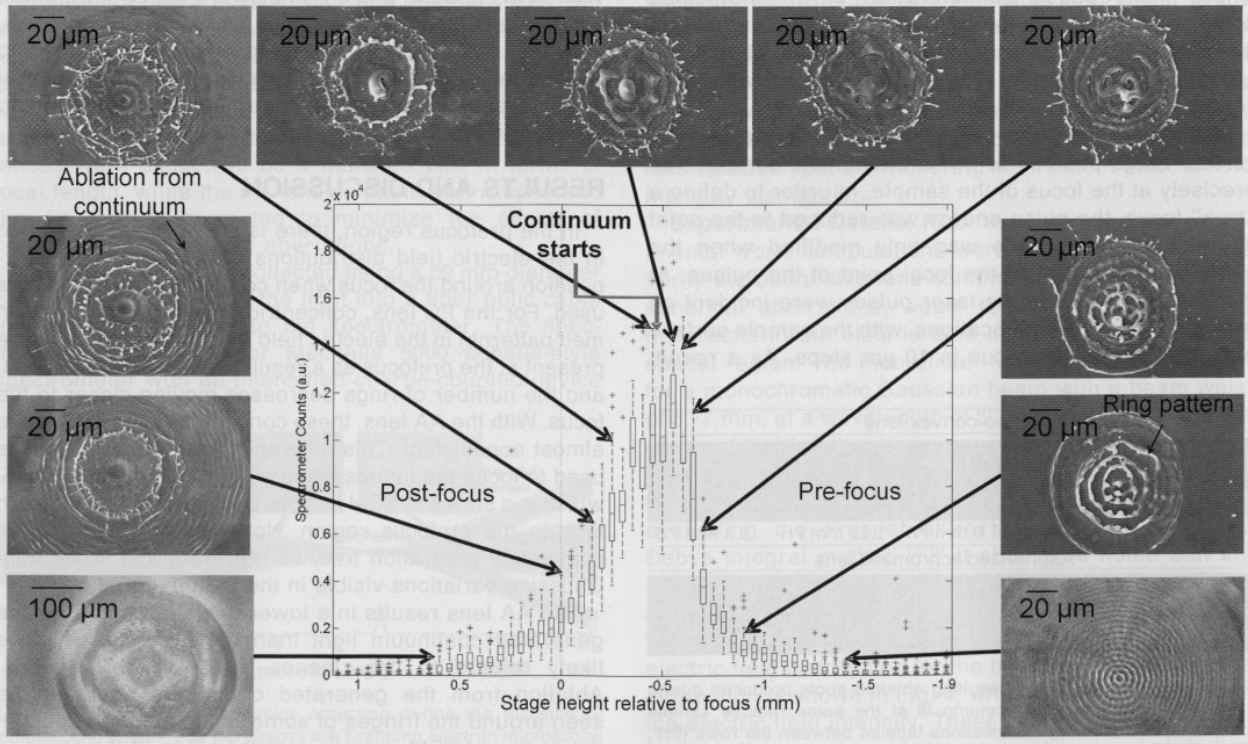

FIG. 8. LIBS and ablation SEM images for a PC lens with a 40 mm focal length.

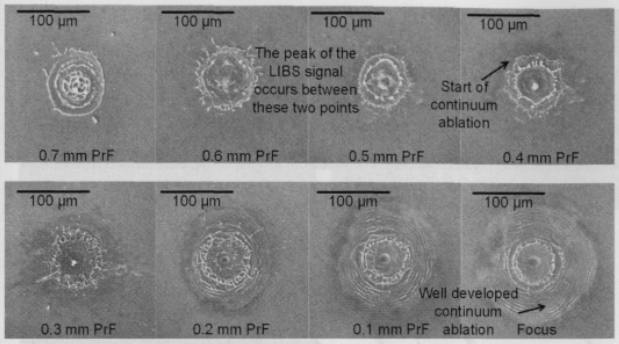

FIG. 9. SEM images of the resulting ablation spots approaching the focus, produced using the PC lens during LIBS data collection.

there is a decrease in the LIBS signal as the ablation from the generated continuum begins. The general shape of the plot can be described starting from the prefocus region (moving right to left):

(1) The LIBS signal increases with fluence (smaller spot size) approaching the focus.
(2) Once the peak intensity is high enough to generate an air plasma and directed continuum light, two processes decrease the LIBS signal.
   (a) Air plasma formation robs some of the pulse energy (lower fluence).
   (b) The directed continuum light, which also produces a LIBS signal, begins to expand in the prefocus region, increasing to total ablation spot size (lowering the fluence), and therefore the LIBS signal decreases.
(3) Enhanced expansion of continuum light continues beyond the focus, leading to a quick and continual decline in LIBS signal.

The onset of ablation from continuum generation can be better seen in another set of SEM images shown in Fig. 9. From these images it is evident that ablation from the continuum light starts around 0.4 mm prefocus. Notice that ablation from the continuum is well developed by the time the pulses reach the focus, leading to a much larger ablation spot than would occur without the continuum generation. This occurs even as the center ablation region following the normal focusing pattern continues to decrease in diameter. A byproduct of the prefocus continuum expansion is that the minimum ablation spot size actually occurs before the focus. This minimum spot size for this set of experiments was about 0.5 mm prefocus. This is also where the peak LIBS signal occurs (see Fig. 8) because it is the location of maximum fluence. At focus, two ablation patterns are visible. The inner pattern is from the normal focusing of the pulses, and the outer pattern is ablation from the continuum light. Since continuum generation from the AA lens does not expand as quickly as from the PC lens, the peak LIBS signal (see Fig. 7) is shifted closer to the focus.

While it may be expected that the aberration-corrected AA lens would have a simpler LIBS signal dependence when compared with the PC lens, the dependence was unexpectedly even more complex. Figure 10 depicts the LIBS signal as a function of sample location relative to the focus, along with the corresponding SEM ablation spot images, for the AA lens. Although the lens is designed to reduce spherical aberrations, it is not a

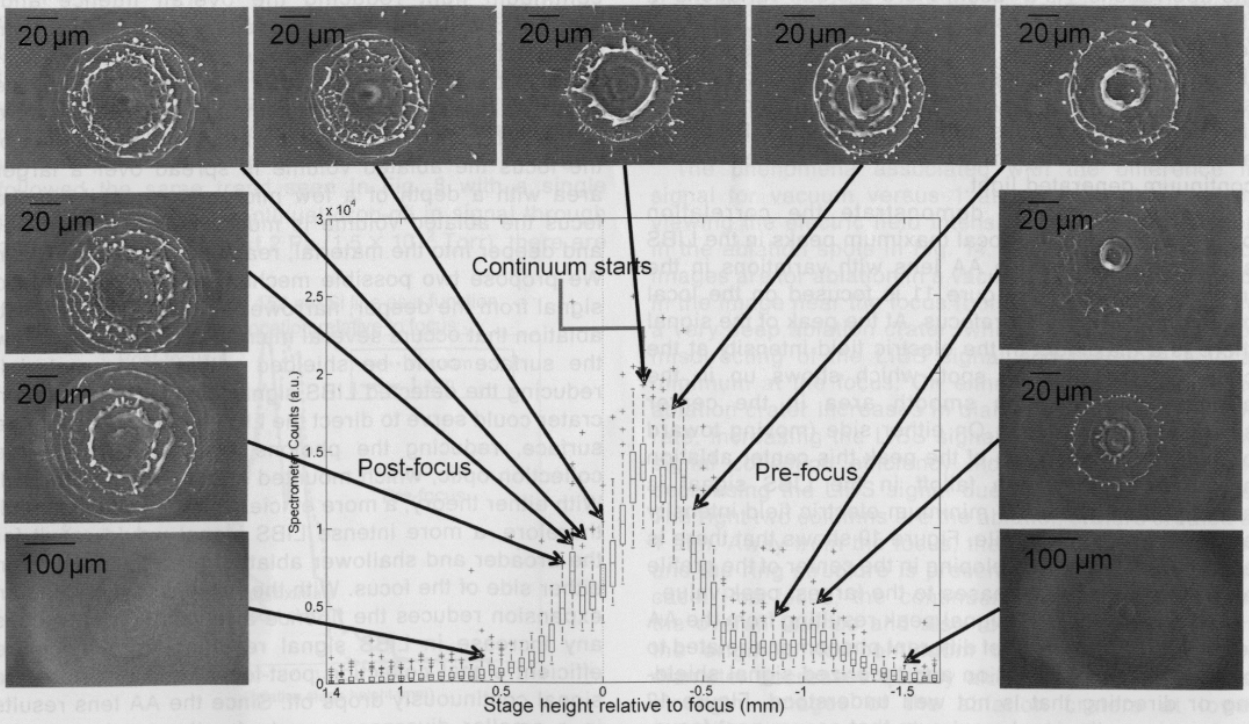

FIG. 10. LIBS and ablation SEM images for a 40 mm focal length AA lens.

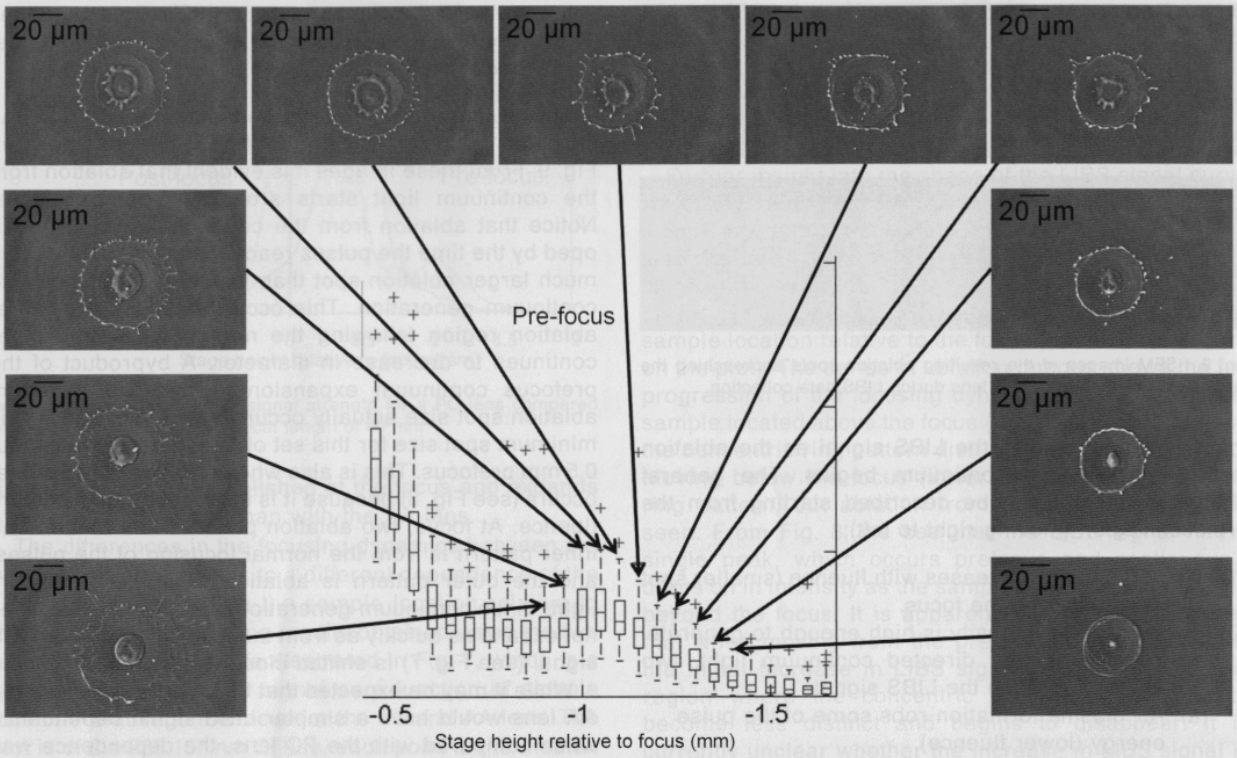

FIG. 11. LIBS and ablation SEM image for a 40 mm focal length AA lens showing the correlation between local maximum and minimum and the closing and opening of the local electric magnetic fields as imprinted using the ablation spots.

perfect achromatic asphere, and with the broadband spectrum from the laser it does not completely eliminate the aberrations. As a result, there are still variations in the electric field intensity distribution as a function of focus. The largest peak in Fig. 10, which corresponds to the similar peak produced with the PC lens, occurs at the same location where ablation from continuum generation begins. This results in a decline in the LIBS signal and an ablation region that can be attributed to this continuum generated light.

Figures 11 and 12 demonstrate the correlation between the other two local maximum peaks in the LIBS signal observed for the AA lens with variations in the intensity distribution. Figure 11 is focused on the local maximum that occurs prefocus. At the peak of the signal there is a maximum in the electric field intensity at the center of the ablation spot, which shows up in the ablation pattern as a smooth area in the center surrounded with a ring. On either side (moving toward or away from the focus) of the peak this center ablation area closes up and a falloff in the LIBS signal is accompanied by a local minimum electric field intensity at the center of the profile. Figure 10 shows that there is a similar maximum developing in the center of the profile as the LIBS signal increases to the largest peak value.

The post-focus LIBS signal peak resulting from the AA lens (Fig. 10) is a result of different phenomena related to both continuum generation and theorized signal shielding or directing that is not well understood. Figure 12 focuses in on the local maximum that occurs post-focus. The shape of the LIBS signal curve in this region comes from two competing processes. The first process, discussed previously, originates from the expansion of continuum light reducing the overall fluence and, therefore, reducing the LIBS signal. This continuum expansion, however, does not explain the local maximum. Although not well understood at this time, we postulate that the local maximum is related to the nature of the ablated volume near the focus. On either side of the focus the ablated volume is spread over a larger area with a depth of a few micrometers, while at the focus the ablated volume is much smaller in diameter and deeper into the material, reaching as deep as 8 µm. We propose two possible mechanisms for the reduced signal from the deeper, narrower ablation craters. First, ablation that occurs several micrometers or more below the surface could be shielded with the top material, reducing the detected LIBS signal. Second, the ablation crater could serve to direct the LIBS signal normal to the surface, reducing the photons that would reach the collection optic, which mounted about 45° off of normal. With either theory, a more efficient signal collection and, therefore, a more intense LIBS signal would result for the broader and shallower ablation area that occurs on either side of the focus. With the PC lens, the continuum expansion reduces the fluence at a rate that outweighs any increase in LIBS signal resulting from the more efficient signal collection post-focus, and therefore the signal continuously drops off. Since the AA lens results in a smaller divergence angle for the continuum, the peak below the focus begins to form but is then

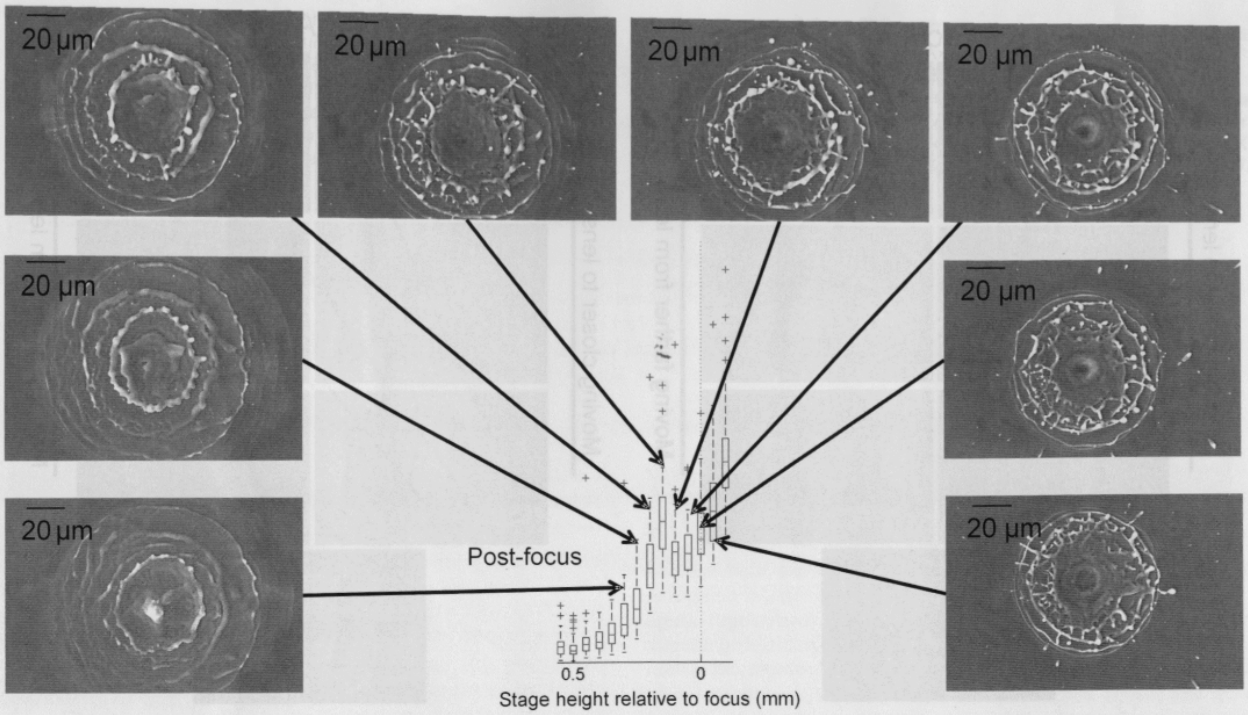

FIG. 12. LIBS and ablation SEM image for a 40 mm focal length AA lens showing the correlation between local maximum and minimum and interplay between ablation efficiency from a more uniform ablation moving post-focus and an increased spot size from continuum expansion.

outweighed by the continuum expansion, leading to a nonsymmetry around the focus.

In order to further test the theory of a local minimum in the LIBS signal near the focus, experiments were completed to compare the LIBS signal as a function of sample location relative to the focus at 1 atm versus 2 Pa (1.5×10^{-2} Torr) using the PC lens. Figure 13 is a plot of the LIBS signal strength as a function of sample location with the sample inside a vacuum chamber. For the 1 atm data set, the sample was in the vacuum chamber with the vacuum pump disconnected. At 1 atm the LIBS signal followed the same trend seen in Fig. 8 with a single prefocus peak and a continual drop-off in signal through and beyond the focus. At 2 Pa (1.5×10^{-2} Torr), there are

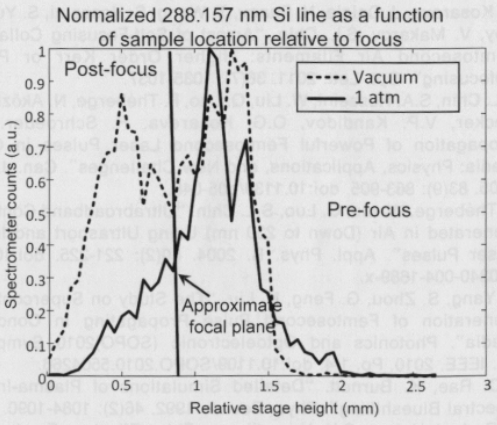

FIG. 13. Comparison of LIBS signal strength as a function of focus for a PC lens in open air versus in a vacuum.

now two peaks of similar magnitude with a local minimum at the focus. This local minimum in the LIBS signal, occurring without significant continuum generation, is likely due to either shielding or signal misdirecting near the focus discussed previously. The slightly lower post-focus peak could be from the limitation in the vacuum system sustaining pressures only as low as 2 Pa (1.5×10^{-2} Torr), allowing the formation of a small amount of continuum. It is also possible that the difference in peaks could be from the difference in electric field intensity distributions on either side of the focus.

The phenomena associated with the difference in signal for vacuum versus 1 atm can be observed by viewing the electric field intensity distributions as seen in the ablation spots in Fig. 14. The left two columns of images are for ablation in a vacuum. Notice the dark spot in the image near the focus (bottom image). This is from a very deep ablation crater, which leads to shielding or misdirecting of the LIBS signal and therefore a local minimum at the focus. On either side of the focus the ablation crater increases in diameter at about the same rate, increasing the LIBS signal to a peak value as the signal collection efficiency increases, and eventually decreasing the LIBS signal due to the drop in fluence. The right two columns are the ablation craters created at 1 atm. Away from the focus, the ablated area increases and the ring structure is present, similar to the vacuum case. Post-focus, the continuum expansion decreases the overall fluence and also robs enough energy from the original, non-continuum beam that the ablated diameter decreases quickly along with the LIBS signal strength. Images of the ablation craters at lower magnifications reveal the larger ablation crater from the expanding continuum seen in previous images.

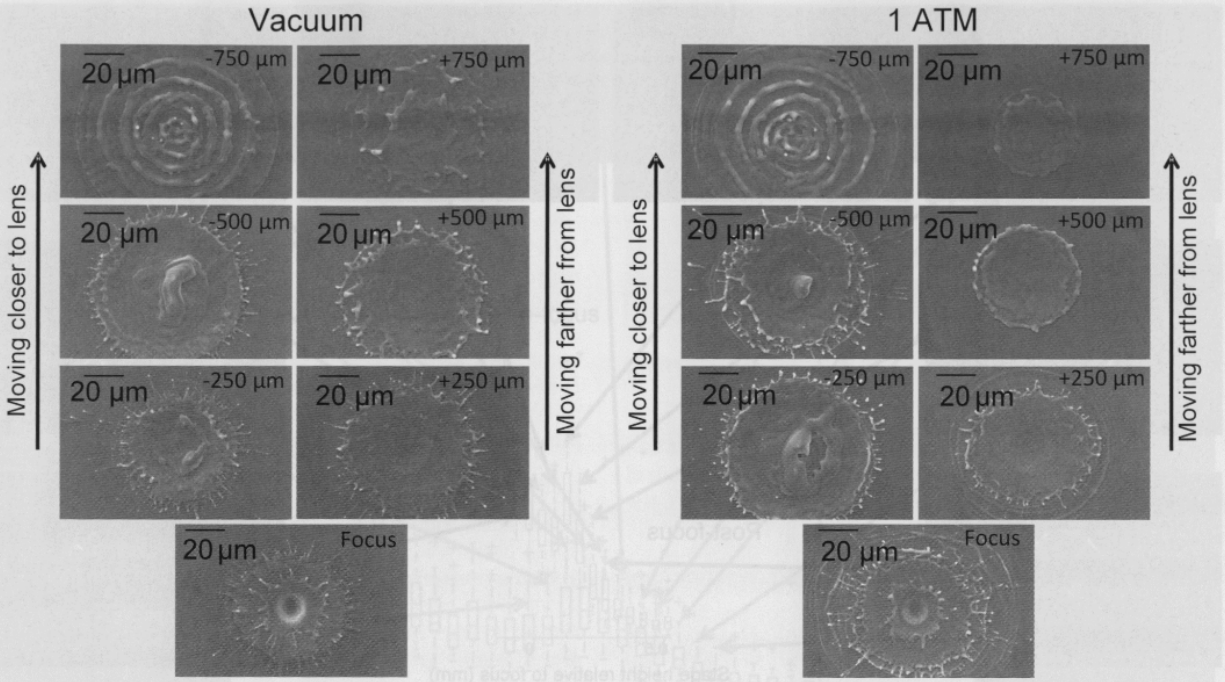

FIG. 14. SEM images of ablation spots created during LIBS signal collection for (left two columns) vacuum, and (right two columns) 1 atm. For each set the bottom image is near the focus and the number in the upper right corner of each image gives the distance the sample surface was from the focus for the corresponding ablation spot. Negative numbers represent the distance from the focus moving toward the lens (prefocus) and positive numbers represent the distance from the focus moving away from the lens (post-focus).

CONCLUSIONS

This work presents, to our knowledge, the first attempt to understand the complex dynamics that result when focusing femtosecond laser radiation in air, and it shows how the intricate electric field intensity distributions affect the LIBS signals. This work demonstrates that with femtosecond laser pulses, concentric ring variations in the electric field intensity distribution in the prefocus region as a result of focusing using a lens with aberrations become frozen in the sample surface. The predominant effects on the LIBS signal strength originate from air plasma/continuum generation, diminishing the energy per pulse and effectively lowering the fluence due to an increase of the total divergence angle in near and post-focus regions. Lens aberrations do affect the LIBS signal even with an aspherized achromatic lens in that a larger LIBS signal can be collected when there is a maximum at the center of the focused profile. This research explains for the first time why there is widely varying data obtained by various LIBS research groups. In order to allow one to extract more quantitative information with LIBS, the precise parameters (lens/beam combination, atmosphere, sample location relative to the focus, etc.) will need to be available for research at various facilities; moreover, laser radiation parameters need to be well characterized and monitored continuously.

ACKNOWLEDGMENTS

This work has been supported by a Multidisciplinary University Research Initiative (MURI) No. W911NF-06-1-0446, Grant Assistance in Areas of National Need (GAANN) No. P200A070344, and a grant through the Nebraska Center for Energy Sciences Research (NCESR) with funds provided by Nebraska Public Power District (NPPD) to the University of Nebraska—Lincoln (UNL) No. 4200000844.

1. P. Bowlan, P. Gabolde, R. Trebino. "Directly Measuring the Spatio-Temporal Electric Field of Focusing Ultrashort Pulses". Opt. Express. 2007. 15(16): 10219-10230.
2. P. Bowlan, P. Gabolde, M.A. Coughlan, R. Trebino, R.J. Levis. "Measuring the Spatiotemporal Electric Field of Ultrashort Pulses with High Spatial and Spectral Resolution". J. Opt. Soc. Am. B. 2008. 25(6): A81-A92. doi:10.1364/JOSAB.25.000A81.
3. M. Rodriguez, R. Bourayou, G. Méjean, J. Kasparian, J. Yu, E. Salmon, A. Scholz, B. Stecklum, J. Eislöffel, U. Laux, A.P. Hatzes, R. Sauerbrey, L. Wöste, J.P. Wolf. "Kilometer-Range Nonlinear Propagation of Femtosecond Laser Pulses". Phys. Rev. E. 2004. 69(3): 036607. doi:10.1103/PhysRevE.69.036607.
4. O. Kosareva, J. Daigle, N. Panov, T. Wang, S. Hosseini, S. Yuan, G. Roy, V. Makarov, S.L. Chin. "Arrest of Self-Focusing Collapse in Femtosecond Air Filaments: Higher Order Kerr or Plasma Defocusing". Opt. Lett. 2011. 36(7): 1035-1037.
5. S.L. Chin, S.A. Hosseini, W. Liu, Q. Luo, F. Théberge, N. Aközbek, A. Becker, V.P. Kandidov, O.G. Kosareva, H. Schroeder. "The Propagation of Powerful Femtosecond Laser Pulses in Optical Media: Physics, Applications, and New Challenges". Can. J. Phys. 2005. 83(9): 863-905. doi:10.1139/p05-048.
6. F. Théberge, W. Liu, Q. Luo, S.L. Chin. "Ultrabroadband Continuum Generated in Air (Down to 230 nm) Using Ultrashort and Intense Laser Pulses". Appl. Phys. B. 2004. 80(2): 221-225. doi:10.1007/s00340-004-1689-x.
7. L. Yang, S. Zhou, G. Feng, K. Liu. "The Study on Supercontinuum Generation of Femtosecond Pulse Propagating in Condensed Media". Photonics and Optoelectronic (SOPO)2010 Symposium on. IEEE. 2010. Pp. 1-4. doi:10.1109/SOPO.2010.5504266.
8. S.C. Rae, K. Burnett. "Detailed Simulations of Plasma-Induced Spectral Blueshifting". Phys. Rev. A. 1992. 46(2): 1084-1090.
9. J. Park, J.-H. Lee, C.H. Nam. "Laser Chirp Effect on Femtosecond Laser Filamentation Generated for Pulse Compression". Opt. Express. 2008. 16(7): 4465-4470.

10. A. Parkes, A.J. Tate, D. Schumacher. "Plasma Formation and Self-Focusing in Continuum Generation". Ohio State University: 2003. http://www.physics.ohio-state.edu/~reu/03reu/REU2003reports/Parkes_final.pdf [accessed Nov 18, 2013].
11. J. Schiffern, D. Doerr, D.R. Alexander. "Optimization of Collinear Double-Pulse Femtosecond Laser-Induced Breakdown Spectroscopy of Silicon". Spectrochim. Acta, Part B. 2007. 62(12): 1412-1418. doi:10.1016/j.sab.2007.10.042.
12. C. Parigger, Y. Tang, D.H. Plemmons, J.W.L. Lewis. "Spherical Aberration Effects in Lens-Axicon Doublets: Theoretical Study". Appl. Opt. 1997. 36(31): 8214-8221.
13. C.G. Parigger. "Laser-Induced Breakdown in Gases: Experiments and Simulation". In: A.W. Miziolek, V. Palleschi, I. Schechter, editors. Laser-Induced Breakdown Spectroscopy. Cambridge, UK: Cambridge University Press, 2006. 1st ed. Pp. 171-193. doi:10.1017/CBO9780511541261.005.